Journal of Thermal Analysis and Calorimetry (2025) 150:15407–15419
https://doi.org/10.1007/s10973-025-14729-0

Comprehensive investigation of fractional jeffrey-type graphene-based nanofluid flow: significance of magnetic field, porosity, and mittag–leffler function

Qasim Ali[1] · Muhammad Amir[2] · Muhammad Farman[3,4,9] · Ahmed Sayed M. Metwally[5] · Hijaz Ahmad[6,7,8]

Received: 13 January 2025 / Accepted: 14 August 2025 / Published online: 15 October 2025

Abstract
The nanofluid's thermal potential is remarkable and provides many dynamical applications in nuclear cooling, extrusion processes, solar collectors, thermal systems, and heating and cooling devices. Due to these motivations, this research examines an unsteady electrically conducting free convective Jeffrey-type nanofluid (graphene nanoparticles distributed in polyvinyl alcohol (PVA)/water) flow over a heated moving plate in a porous medium. The key motivation of recent work is to evaluate how fractional calculus, especially the newly developed Prabhakar fractional operator, having the Mittag–Leffler function in its kernel with three different parameters, can more precisely explain the memory as well as hereditary characteristics of nanofluid (NF) flows in complex media, thereby contributing a deeper perception into energy transport mechanisms. The fractional governing equations are designed by employing the Prabhakar derivative and solved with the Laplace technique. The key findings show that the momentum and temperature profiles rise with larger estimations of the solar radiation parameter. The velocity and thermal fields go down while enlarging the Prandtl number. Among base fluids, water-based NF shows higher thermal behaviour as compared to PVA-based nanofluid. These results can be used to advance the efficiency of heat exchangers, solar collectors, photovoltaic–thermal networks, and other industrial and engineering processes by increasing heat transfer and energy absorption.

Keywords Jeffrey-type MHD free convection nanofluid · Porous medium · Solar energy · Prabhakar fractional derivative · Laplace transform

✉ Qasim Ali
aliqasim829@gmail.com

Muhammad Amir
amirramzan423@gmail.com

Muhammad Farman
farmanlink@gmail.com

Ahmed Sayed M. Metwally
dalsayed@ksu.edu.pk

Hijaz Ahmad
hijaz.ahmad@neu.edu.tr

[1] Research Center of Applied Mathematics, Khazar University, Baku, Azerbaijan

[2] Department of Mathematics, University of Engineering and Technology, Lahore, Pakistan

[3] Faculty of Arts and Science, Department of Mathematics, Near East University, 99138 Nicosia, Turkey

[4] Research Center of Applied Mathematics, Khazar University, 11451 Baku, Azerbaijan

[5] Department of Mathematics, College of Science, King Saud University, 11451 Riyadh, Saudi Arabia

[6] Operational Research Center in Healthcare, Near East University, Nicosia/TRNC, 99138 Mersin 10, Turkey

[7] Department of Mathematics, College of Science, Korea University, 145 Anam-Ro, Seongbuk-Gu, Seoul 02841, South Korea

[8] Department of Technical Sciences, Western Caspian University, Baku 1001, Azerbaijan

[9] Jadara University Research Center, Jadara University, Irbid, Jordan

Introduction

Fractional calculus deals with the simulation of several physical phenomena by various methods. Retardation processes, biophysics, electrochemistry, engineering processes, viscoelasticity, mechatronics, bioengineering, and dynamical procedures are all examples of realistic fractional calculus applications [1]. The phenomenon involving the local and non-local kernels may be effectively handled with the assistance of the fractional technique. In fractional calculus, two non-integer (fractional) derivative methods—Caputo and Fabrizio, Atangana, and Baleanu—are significant and are considered by several investigators.

Fractional calculus contains many different kinds of functions. The Mittag–Leffler function (MLF) is very crucial among these functions. Tilak Raj Prabhakar developed an innovative non-integer operator called the Prabhakar operator by incorporating the MLF, having three different parameters. The fundamental properties of the Prabhakar operator with the MLF were discussed in [2]. By using the Prabhakar operator, the fractional-based mathematical model of viscoelasticity was studied in [3]. Alsharif et al. [4] studied the flow process along with a fractional operator using coaxial vertical tubes on a hybrid nanofluid (HNF). They realised that when the volume concentration increased, the velocity profile exhibited a declining trend. Rehman et al. [5] examined the application of the Prabhakar derivative in the Maxwell fluid flow mechanism with the influence of Newtonian heating. With the use of the MLF, they obtained the results as well as compared them with the ordinary model. Using the Prabhakar operator, a fractional mathematical problem including two distinct kinds of NFs and comparing their thermal behaviour through a channel was studied in [6]. They investigated that the temperature field is enhanced by greater fractional constraint values. Khan et al. [7] showed how to use the Prabhakar-based model to demonstrate a flow in Jeffrey fluid. In their investigation, they observed an increase in the velocity that aligned with the fractional parameters. Some current investigations on fractional NFs can be studied in [8–10] and their references.

There is no disputing that sustainable energy production is a hot subject in the whole world due to human society's fast progress; there is a significant need to reduce contamination of the environment and address global energy challenges. Solar energy is the greatest reliable source of free energy with low environmental effects on human beings. The most recent investigations on solar energy, as well as fresh research paths from researchers, have discovered that NFs may boost solar collection with thermal transmission rates. Hamzaoui et al. [11] considered the thermal effect of carbon nanotubes caused by an inclined plate with Lorentz force to boost the thermal system of water and human blood base fluids by using the Prabhakar derivative. They considered the mixed convection and solved the problem by the integral transform. Maatoug et al. [12] examined the fractionalised Casson fluid with the Laplace transform method and applied Caputo–Fabrizio derivative for fractional phenomena. They used sodium alginate and water as base fluids with an interface of silver and titanium dioxide hybrid nanofluids. The profile of velocity was shown to increase with the Grashof number.

Raza et al. [13] investigated the Prabhakar-based mixed convection HNF fractional model along with a magnetic field and an oscillating vertical plate. They considered the carboxymethyl cellulose and blood-based fluid model with single- and multi-walled carbon nanotubes to discuss the comparative thermal characteristics of base materials and carbon nanotubes. Ali et al. [14] studied Prabhakar-based fractional HNF containing ferric oxide and zinc oxide, and an external heat source was used to boost the rate of heat transfer. A fractional model which represents the thermal characteristics of a Brinkman-type HNF with mixed convection effects by using the Prabhakar scheme was examined by Qadir et al. [15]. They considered that the magnetic force and the oscillating plate initiate the flow. Acharya et al. [16] discussed the HNF to advance the proficiency of solar structures. Sheikh et al. [17] discussed second-grade fluid analytically. Kataria et al. [18] investigated the Soret effect on the MHD flow in a vertical channel. The solution for non-integer order Navier–Stokes equations using a novel semi-analytical approach was examined in [19]. The fractional approach generalises the ordinary derivative that uses non-integer differentiation. Researchers have taken special care of the fractional derivative because of its generalised characteristics, which make it a powerful tool for describing heat and mass transport processes. Sene [20] examined a fractionalised viscous fluid model with Newtonian heating employing the Caputo fractional operator. Chu et al. [21] obtained the viscous NF model's analytical solution, represented by a constant non-local proportional Caputo fractional operator. Acharya [16] examined the thermal properties of HNFs through a channel analytically. Song et al. [22] investigated the effects of copper NPs flowing through water on a fast-heating surface. The benefits of solar energy using Sutterby HNF in solar systems subjected to expanded sheets were investigated in [23]. The effects of NPs in diverse fluid models with different geometries were discussed in the latest studies [24–27].

In the light of these crucial considerations, NFs captured the scientific community's attention because of their importance in solar systems and energy transfer advancement. In reality, such NF flows have numerous applications in engineering fields, including transformer oil cooling, solar water heating, industrial cooling, and heating chambers, advancements in diesel engine performance, vehicle engine cooling, fuel savings for electricity-producing plants, cooling processes of electronic chips, refrigerant, and several

others. At present, the application of NPs is a hot topic for research among several researchers. The ability to synthesise NPs of changing materials, shapes, and sizes and efficiently accumulate them into complete structures has a significant impact on development in several areas. Furthermore, significant base fluids in which NPs are usually suspended include ethylene glycol, water, and motor oil. Bilal et al. [28] studied MHD Brinkman-type NF over a vertical sheet with slip conditions, thermal radiation, and heat absorption/generation effects.

The Prabhakar derivative is applied because of its capacity to model complex physical processes with non-local and memory effects with greater precision than classical and other non-integer order derivatives. Unlike classical and even some other fractional approaches (such as Caputo–Fabrizio or Caputo), the Prabhakar operator incorporates a three-parameter Mittag–Leffler function in its kernel, which provides greater flexibility in modelling real-world processes that have various relaxation and retardation effects. Its three-parameter kernel captures a wide range of relaxation and diffusion behaviours, which makes it ideal to study NF flow in porous media. This improved modelling ability is especially beneficial for enhancing the thermal investigation of industrial heat exchangers, solar collectors, photovoltaic thermal frameworks, and energy-efficient devices, where precise control of heat exchange is necessary [29].

To the best of the author's knowledge, no prior study has examined the fractional modelling of MHD Jeffrey-type nanofluid (graphene NPs distributed in PVA/water), over a moving heated plate, entrenched in a porous medium, by using the Prabhakar fractional technique. Whereas the previous works have studied the fractional NFs with several base fluid–NPs combinations. In general, they have been restricted to classical derivatives, simpler geometries, or traditional NPs such as $\left(Cu, Al_2O_3, TiO_2\right)$.

The current study is unique in three significant objectives:

- Graphene NPs, which have higher stability and thermal conductivity than conventional NPs, are used in PVA/water.
- Combination of moving effects together with NF and porous medium features in a fractional framework.
- Use of the newly presented Prabhakar derivative, which more efficiently captures hereditary and memory effects than Caputo–Fabrizio, Caputo, or Atangana–Baleanu techniques.

These contributions increase the understanding of hydrodynamic fractional NF flows in complex physical situations and are appropriate to coating technologies, thermal management, and energy systems using graphene-based nanofluids.

Formulation of the flow model based on prabhakar derivative

Consider a free convective electrically conducting flow of a Jeffrey-type nanofluid (graphene NPs distributed in PVA/water) entrenched in a porous medium on a moving heating plate. We use a Cartesian coordinate system (x, z), where x is the coordinate along the plate, and z is normal to the plate. A uniform magnetic field B_0 is used normal to the $x-$ axis (i.e. along the z-direction). Initially, $(t \le 0)$. The fluid as well as the plate are in a relaxation position and at a uniform ambient temperature ϕ_∞. For $t > 0$, the temperature and velocity of the plate are elevated to $\phi_\infty + \phi_w\left(1 - ae^{-bt}\right)$ and $U_0 g(t)$, respectively, where ϕ_w, a, b are constants. The flow may rotate with angular velocity Ω. Temporal memory effects are included by the Prabhakar fractional derivative acting on time-dependent terms. By using Boussinesq approximation along the above assumptions, the governing equations for the MHD rotating Jeffrey-type NF for free convective flow are [30, 31]:

$$\frac{\xi_1 \mu_{nf}}{\left(1+\lambda_1\right)k}\left(\lambda_2 \frac{\partial v}{\partial t} + v\right) - \frac{\mu_{nf}}{\left(1+\lambda_1\right)}\frac{\partial^2 v}{\partial z^2}\left(1 + \lambda_2 \frac{\partial}{\partial t}\right) + \rho_{nf}\left(\frac{\partial v}{\partial t} + 2\Omega i v\right) - g\left(\rho\beta_\phi\right)_{nf}\left(\phi - \phi_\infty\right) + \sigma B_0^2 v = 0, \tag{1}$$

$$\left(\rho C_p\right)_{nf}\frac{\partial \phi}{\partial t} = K_{nf}\frac{\partial^2 \phi}{\partial z^2} - \frac{\partial q_r}{\partial z} \tag{2}$$

The initial and boundary conditions are.

$$v(z,0)=0,\ \phi(z,0) = \varnothing_\infty, \tag{3}$$

$$v(0,t) = U_0 g(t), \phi(0,t) = \phi_\infty + \phi_w\left(1 - ae^{-bt}\right), \tag{4}$$

$$v(\infty,t) = 0, \phi(\infty,t) = \phi_\infty. \tag{5}$$

Symbol		Quantity	Unit
v	:	Velocity	$(\mathrm{m\ s^{-1}})$
t	:	Time	(s)
ϕ	:	Temperature	(K)
K_{nf}	:	Thermal conductivity of nanofluid	$(\mathrm{W\ m^{-1}\ K^{-1}})$
k	:	Permeability of porous medium	(L)
ϕ_∞	:	Constant temperature	(K)
Gr	:	Grashof number	$(-)$
Ha	:	Hartmann number	$(-)$
Pr	:	Prandtl number	$(-)$
q	:	Laplace transform variable	$(-)$
r	:	Rotation parameter	$(-)$
C_p	:	Particular heat at continuous pressure	$(\mathrm{J\ kg^{-1}\ K^{-1}})$
G	:	Gravitational acceleration	$(\mathrm{m\ s^{-2}})$

Symbol		Quantity	Unit
C_f	:	Skin friction	(−)
Nu	:	Nusselt number	(−)
q_r	:	Radiation heat flux	(W m^{-2})
K_s, K_f	:	Thermal conductivities of the solid and base fluids	(W m^{-1} K^{-1})
K_1	:	Absorption coefficient	(m^2 mol^{-1})
$1/k$	:	Permeability parameter	(−)
Rd	:	Radiation parameter	(−)
$H(t)$	:	Heaviside function	(−)

Greek Letters:

μ_{nf}	:	Dynamic viscosity of nanofluid	(Pa-s)
(α, β, γ)	:	FractionalparametersforPrabhakar Derivative	(−)
ξ_1	:	Porosity parameter	(L)
β_ϕ	:	Volumetric coefficient of expansion	(−)
ρ_{nf}	:	Density of nanofluid	(kg m^{-3})
σ	:	Electrical conductivity	Siemens per meter (S m^{-1})
ρ_f, ρ_s	:	Density of fluid and solid nanoparticles	(kg m^{-3})
φ	:	The volume fraction of nanofluid	(−)
λ_1	:	Viscosity parameter for nanofluid	(−)
λ_2	:	Second-grade nanofluid parameter	(−)
$(\rho\beta_\phi)_{nf}$	:	Thermalexpansioncoefficientof Nanofluid	(K^{-1})
β_s, β_f	:	Volumetric coefficient of expansion for solid nanoparticles and base fluids	(K^{-1})
σ^*	:	Stefan–Boltzmann constant	(−)
λ	:	dimensionless material parameter	(−)

Note: This (−) signifies the dimensionless quantity.

${}^{C}\mathfrak{D}^{\gamma}_{\alpha,\beta,\alpha}$	:	Prabhakar time fractional derivative
NPs	:	Nanoparticles
NF	:	Nanofluid
MHD	:	Magnetohydrodynamics
PVA	:	Polyvinyl alcohol
HNF	:	Hybrid nanofluid

This model comprises the second-grade NF as a special case (for $\lambda_1 = 0$) and the Newtonian NF (for $\lambda_1 = \lambda_2 = 0$).

Subsequently, the relations $\mu_{nf}, \rho_{nf}, (\rho C_p)_{nf}, (\rho\beta_\varnothing)_{nf}$ are described as [32, 33]

$$(\rho C_p)_{nf} = (\rho C_p)_s \varphi + (1-\varphi)(\rho C_p)_{f,} \tag{6}$$

$$(\rho\beta)_{nf} = (\rho\beta)_s \varphi + (1-\varphi)(\rho\beta)_f, \tag{7}$$

$$\mu_{nf} = \mu_f (1-\varphi)^{-2.5}, \tag{8}$$

$$(\rho)_{nf} = (\rho)_s \varphi + (1-\varphi)(\rho)_f, \tag{9}$$

$$\frac{K_{nf}}{K_f} = \frac{2(\varphi K_s - \varphi K_f) + K_s + 2K_f}{(\varphi K_s - \varphi K_f) + K_s + 2K_f}. \tag{10}$$

Rosseland estimation and radiation thermal flux [34, 35] are defined as

$$\frac{3K_1}{4\sigma^*} = -\frac{1}{q_r}\frac{\partial \phi^4}{\partial z}. \tag{11}$$

Furthermore, due to temperature variations, we considered that the flow is sufficiently small. Ignoring higher-order terms ultimately yields.

$$\phi^4 \approx -(3\phi_\infty^4 - 4\phi\phi_\infty^3). \tag{12}$$

Using Eqs. (11)–(12) in Eq. (2), we have

$$\frac{(\rho C_p)_{nf}}{K_f}\frac{\partial \phi}{\partial t} = \frac{\partial^2 \phi}{\partial z^2}\left[\frac{K_{nf}}{K_f} + \frac{16\sigma^* \phi_\infty^3}{3K_f K_1}\right]. \tag{13}$$

Introducing the below dimensionless variables.

$$\phi^* = \frac{\phi(y.t) - \phi_\infty}{\phi_w}, z^* = \frac{zU_0}{\vartheta}, v^* = \frac{v}{U_0}, t^* = \frac{tU_0^2}{\vartheta}. \tag{14}$$

Applying Prabhakar derivative and the above dimensionless parameters in Eq. (14), the energy Eq. (13) and momentum Eq. (1) with corresponding conditions (3)–(5) take the form as

$$\frac{\partial^\delta v}{\partial t^\delta} + \frac{B_2}{K(1+\lambda_1)}\left(1 + \lambda_2\frac{\partial^\delta}{\partial t^\delta}\right)v - \frac{B_1}{1+\lambda_1}\left(1 + \lambda\frac{\partial^\delta}{\partial t^\delta}\right)\frac{\partial^2 v}{\partial z^2} + 2irv - \mathrm{Gr}\psi + \frac{\mathrm{Ha}}{B_3}v = 0, \tag{15}$$

$$\frac{\partial^\delta \phi}{\partial t^\delta} - B_4\frac{\partial^2 \varnothing}{\partial z^2} = 0. \tag{16}$$

It is important to note that the symbol. $\frac{\partial^\delta}{\partial t^\delta} = {}^{C}\mathfrak{D}^{\gamma}_{\alpha,\beta,\alpha}$ denotes the Prabhakar derivative and is expressed [33] as

$${}^{C}\mathfrak{D}^{\gamma}_{\alpha,\beta,\alpha} h(t) = E^{-\gamma}_{\alpha,n,-\beta,\alpha} h^n(t) = e^{-\gamma}_{\alpha,n,-\beta}(\alpha;t) * h^n(t)$$

$$= \int_0^t (t-\tau)^{n-\beta-1} E^{-\gamma}_{\alpha,n,-\beta}(\alpha(t-\tau)^{\alpha}) h^{n}(\tau) d\tau, \tag{17}$$

Where $h^{(n)}$ indicates the n^{th} derivative of $h(t) \in AC^{n}(0,b), AC^{n}(0,b)$ shows a real-valued function taking constant derivatives of $(n-1)$ order in the interval $(0,b)$. Furthermore,

$$E^{\gamma}_{\alpha,\beta,\alpha} h(t) = \int_0^t E^{-\gamma}_{\alpha,\beta}\left(\alpha(t-\tau)^{\alpha}\right)(t-\tau)^{\beta-1} h(\tau) d\tau \tag{18}$$

is the Prabhakar integral with the MLF represented by $E^{\gamma}_{\alpha,\beta}(z_1)$, which is a generalised form of the two-parameter MLF [33]:

$$E^{\gamma}_{\alpha,\beta}(z_1) = \sum_{m=0}^{\infty} \frac{(\gamma) m z^{m}}{m! \Gamma(\alpha m + \beta)}, \tag{19}$$

where.

z_1 is a complex parameter, α, β, and γ are called complex parameters, $\Gamma(\cdot)$ is a Gamma function, and $(\gamma)k$ is the Pochhammer symbol/rising factorial, stated in the form as.

$$(\gamma)j = \gamma(\gamma+1)(\gamma+2)\cdots(\gamma+j-1) for j \geq 1 \text{ and } (\gamma)0 = 1.$$

The Eq. $e^{\gamma}_{\alpha,\beta}(\alpha;t) = t^{\beta-1} E^{\gamma}_{\alpha,\beta}(\alpha t^{\alpha})$ is the Prabhakar kernel. The Laplace operator ${}^{C}\mathfrak{D}^{\gamma}_{\alpha,\beta,\alpha}$ is written as [34]

$$\mathcal{L}\left[{}^{C}\mathfrak{D}^{\gamma}_{\alpha,\beta,\alpha} h(t)\right] = \mathcal{L}\left[h^{m}(t) * e^{-\gamma}_{\alpha,m-\beta}(\alpha;t)\right] = \mathcal{L}\{h^{m}(t)\}\mathcal{L}\left\{e^{-\gamma}_{\alpha,m-\beta}(\alpha;t)\right\}$$

$$= \mathcal{L}\{h^{m}(t)\} s^{\beta-m}(1-\alpha s^{-\alpha})^{\gamma}. \tag{20}$$

The resultant conditions take the form of

$$v(z,0) = 0, \phi(z,0) = 0; t > 1, \tag{21}$$

$$v(0,t) = g(t), \phi(0,t) = \left(1 - ae^{-bt}\right); t > 1, \tag{22}$$

$$v(\infty,t) = 0, \phi(\infty,t) = 0; t > 1, \tag{23}$$

where,

$$\begin{aligned} &\mathrm{Gr} = \frac{g\beta_f \vartheta(\emptyset_w - \emptyset_\infty)}{U_0^3}, \mathrm{Ha} = \frac{\sigma \vartheta B_0^2}{U_0^2 \rho_f}, \frac{1}{k} = \frac{\vartheta \xi_1}{U_0^2 K^*}, \\ &r = \frac{\eth\Omega}{U_0^2}, \lambda = \frac{\lambda_2 U_0^2}{\vartheta}, \ \mathrm{Rd} = \frac{16\sigma \hat{} \emptyset_\infty^3}{16 K_1 K_f}, \mathrm{Pr} = \frac{\vartheta_f}{\beta_f}. \end{aligned} \tag{24}$$

By taking a replacement for the simplicity of the governing equations, as,

$$B_4 = \frac{(l_2 + \mathrm{Rd})}{l_1 \mathrm{Pr}}, B_3 = \varphi\frac{\rho_s}{\rho_f} + (1-\varphi), B_2 == \varphi\frac{(\beta\rho)_s}{(\beta\rho)_f} + (1-\varphi), B_1 == \frac{1}{\left[\varphi\frac{\rho_s}{\rho_f} + (1-\varphi)\right](1-\varphi)^{2.5}},$$

$$l_2 = \frac{2(\varphi K_s - \varphi K_f) + K_s + 2K_f}{(\varphi K_s - \varphi K_f) + K_s + 2K_f}, l_1 = \varphi\frac{(\rho C_p)_s}{(\rho C_p)_f} + (1-\varphi). \tag{25}$$

Solution of the proposed model

Temperature distribution with prabhakar derivative

By using the Laplace transform on Eq. (16) with conditions in Eqs. $(21)_2$–$(23)_2$, and (20), we get

$$q^{\beta}(1-\alpha q^{-\alpha})^{\gamma}\overline{\phi}(z,q) - B_4\frac{\partial^2\overline{\phi}(z,q)}{\partial z^2} = 0. \tag{26}$$

After some calculations and simplifications on Eq. (26), we get

$$\frac{\partial^2\overline{\phi}(z,q)}{\partial z^2} - \frac{q^{\beta}(1-\alpha q^{-\alpha})^{\gamma}}{B_4}\overline{\phi}(z,q) = 0. \tag{27}$$

Equation (27) may be written as

$$\overline{\phi}(z,q) = C_1 e^{z\sqrt{\frac{q^{\beta}(1-\alpha q^{-\alpha})^{\gamma}}{B_4}}} + C_2 e^{-z\sqrt{\frac{q^{\beta}(1-\alpha q^{-\alpha})^{\gamma}}{B_4}}}. \tag{28}$$

The related Laplace domain boundary conditions are

$$\overline{\phi}(0,q) = \frac{1}{q} - \frac{a}{q+b}, \overline{\phi}(\infty,q) = 0. \tag{29}$$

By using conditions (29), the solution of the temperature Eq. (28) is

$$\overline{\phi}(z,q) = \left(\frac{1}{q} - \frac{a}{q+b}\right) e^{-z\sqrt{\frac{q^{\beta}(1-\alpha q^{-\alpha})^{\gamma}}{B_4}}}. \tag{30}$$

Velocity distribution with prabhakar derivative

By application of the Laplace transform on Eq. (15), with conditions in Eqs. $(21)_1$–$(23)_1$, and (20), we get

$$\left[q^{\beta}(1-\alpha q^{-\alpha})^{\gamma} + \frac{B_2}{(1+\lambda_1)K}\left\{1 + \lambda_2 q^{\beta}(1-\alpha q^{-\alpha})^{\gamma}\right\} + 2ir + \frac{\mathrm{Ha}}{B_3}\right]$$

$$\overline{v}(z,q) - \frac{B_1}{(1+\lambda_1)}$$

$$\left[1+\lambda q^{\beta}(1-\alpha q^{-\alpha})^{\gamma}\right]\frac{\partial^2\overline{v}(z,q)}{\partial z^2}-\mathrm{Gr}\,\overline{\phi}(z,q)=0. \tag{31}$$

Equation (31) can be written as(31)

$$\left[1+\lambda q^{\beta}\left(1-\alpha q^{-\alpha}\right)^{\gamma}\right]\frac{B_1}{\left(1+\lambda_1\right)}\frac{\partial^2\overline{v}(z,q)}{\partial z^2}-\left[q^{\beta}\left(1-\alpha q^{-\alpha}\right)^{\gamma}+\frac{B_2}{\left(1+\lambda_1\right)K}\right.$$

$$\left.\left\{1+\lambda_2 q^{\beta}(1-\alpha q^{-\alpha})^{\gamma}\right\}+2\mathrm{ir}+\frac{\mathrm{Ha}}{B_3}\right]\overline{v}(z,q)=-Gr\overline{\phi}(z,q). \tag{32}$$

By using the solution of temperature $\overline{\phi}(z,q)$ in Eq. (32) from Eq. (30), we get

$$\left[1+\lambda q^{\beta}\left(1-\alpha q^{-\alpha}\right)^{\gamma}\right]\frac{B_1}{\left(1+\lambda_1\right)}\frac{\partial^2\overline{v}(z,q)}{\partial z^2}-\left[q^{\beta}\left(1-\alpha q^{-\alpha}\right)^{\gamma}+\frac{B_2}{\left(1+\lambda_1\right)K}\right.$$

$$\left.\left\{1+\lambda_2 q^{\beta}(1-\alpha q^{-\alpha})^{\gamma}\right\}+2\mathrm{ir}+\frac{\mathrm{Ha}}{B_3}\right]\overline{v}(z,q)$$

$$=-Gr\left(\frac{1}{q}-\frac{a}{q+b}\right)e^{-z\sqrt{\frac{q^{\beta}(1-\alpha q^{-\alpha})^{\gamma}}{B_4}}}. \tag{33}$$

The solution of Eq. (33) is

$$\overline{v}(z,q)=C_3e^{z\sqrt{\frac{E}{F}}}+C_4e^{-z\sqrt{\frac{E}{F}}}-\frac{Gr}{F}\left(\frac{1}{q}-\frac{a}{q+b}\right)e^{-z\sqrt{\frac{q^{\beta}(1-\alpha q^{-\alpha})^{\gamma}}{B_4}}}. \tag{34}$$

The corresponding conditions are

$$\overline{v}(0,q)=G(q),\overline{v}(\infty,q)=0. \tag{35}$$

On solving the velocity Eq. (34) with the relevant conditions (35), we have

$$\overline{v}(z,q)=*\,G(q)e^{-z\sqrt{\frac{E}{F}}}+\frac{G}{F}\times\frac{1}{\frac{q^{\beta}(1-\alpha q^{-\alpha})^{\gamma}}{B_4}-\frac{E}{F}}\left[e^{-z\sqrt{\frac{E}{F}}}-e^{-z\sqrt{\frac{q^{\beta}(1-\alpha q^{-\alpha})^{\gamma}}{B_4}}}\right], \tag{36}$$

where,

$$E=(1-\alpha q^{-\alpha})^{\gamma}q^{\beta}+\frac{B_2}{\left(1+\lambda_1\right)K}\left[\left\{1+\lambda_2 q^{\beta}(1-\alpha q^{-\alpha})^{\gamma}\right\}+2\mathrm{ir}+\frac{\mathrm{Ha}}{B_3}\right],$$

$$\mathrm{F}=\frac{B_1}{\left(1+\lambda_1\right)}\left[1+\lambda q^{\beta}(1-\alpha q^{-\alpha})^{\gamma}\right],\ \mathrm{G}=Gr\left(\frac{1}{q}-\frac{a}{q+b}\right).$$

The expressions for the temperature and momentum profile in Eqs. (30) and (36) are too complicated to solve analytically. So, the inverse Laplace transform of these equations can be obtained numerically utilising the Zakian technique. The solutions can be estimated by the Zakian scheme in such a way that [36]:

$$v(z,t)=\frac{t}{3}\sum_{\mathrm{i}=1}^{n}Re\left[\beta_{\mathrm{i}}\overline{v}\left(z,\frac{\alpha_{\mathrm{i}}}{t}\right)\right], \tag{37}$$

where α_{i} and β_{i} are constants, and $Re(.)$ denotes a real part of the function $\overline{v}(z,q)$.

To compare and validate our found numerical results from the Zakarian scheme [36], two other inverse techniques, *i.e.* Stehfest as well as the Tzou algorithm for transformed variable t, are used. To get the numerical solution of energy as well as velocity numerically. Grave Stehfest system [37] is

$$w(\xi,t)=\frac{\ln(2)}{t}\sum_{n=1}^{M}v_{\mathrm{n}}\overline{w}\left(\xi,n\frac{\ln(2)}{t}\right) \tag{38}$$

where M is a non-negative integer, and

$$v_{\mathrm{n}}=(-1)^{\mathrm{n}+\frac{\mathrm{M}}{2}}\sum_{\mathrm{p}=\left[\frac{q+1}{2}\right]}^{\min\left(q,\frac{M}{2}\right)}\frac{p^{\frac{\mathrm{M}}{2}}(2p)!}{\left(\frac{M}{2}-p\right)!p!(p-1)!(q-p)!(2p-q)!}. \tag{39}$$

The Tzou scheme [38] has the form of

$$w(\xi,t)=\frac{e^{4.7}}{t}\left[\frac{1}{2}\overline{w}\left(r,\frac{4.7}{t}\right)+\mathrm{Re}\left\{\sum_{j=1}^{N}(-1)^{\mathrm{k}}\overline{w}\left(r,\frac{4.7+k\pi i}{t}\right)\right\}\right], \tag{40}$$

where i and Re(.) are imaginary units and real portions, and $N>1$ is a natural number.

Results with discussion

This section explains the analytical results of the moving plate with rotating Jeffrey NF that is electrically conductive, computed using the Laplace method. In this problem, the base fluids are water and PVA, and the base fluids are affected by graphene NPs. The plate is moved while the investigation is conducted for temperature and velocity data with $g(t)=H(t), g(t)=t, g(t)=e^{-\omega t}$, and $g(t)=te^{-\omega t}$. The analysis is conducted while varying several physical parameters, like $Pr, Rd, Ha, Gr, \alpha=\beta=\gamma$ in the graphical representation at specified time values of velocity and temperature. Figures 1–7 demonstrate various temperature and velocity variations due to changes in different physical parameters and base fluids, and these figures provide an appreciation perception into the effect of these parameters on both profiles in the system.

The change in temperature and velocity for different Prandtl numbers (Pr) is displayed in Fig. 1. The variations in Prandtl number are associated with thermal diffusivity effects. The decline in both curves is found with the enhancement of Pr. An increased value for Pr decreases both profiles. The heat disseminates more rapidly in the case of enlargement in Pr,

which lessens thermal transfer, as well as velocity phenomena, in the fluid. The Prandtl number governs the dominant mode of thermal transference in a fluid. The domination in heat diffusivity is indicated by the low values of the Prandtl number, meaning that the fluid has more capacity to transmit velocity than heat. Conversely, the value of Pr shows that thermal diffusivity is dominant, indicating that the fluid is more capacitive at transporting heat than velocity.

The effect of radiation parameter (Rd) on both profiles is revealed graphically in Fig. 2. The radiation factor is related to radiative heat transfer development. We see that increasing Rd increases the fluid heat and momentum profiles. Physically, when the radiation rises, thermal buoyancy force decreases, resulting in a thin energy boundary layer, and hence, temperature and velocity increase.

Figure 3 explains the impact of fractional factors (α, β, γ) on both profiles. The fractional parameters are associated with studying the memory effects in fluid motion. We see that both profiles express an increasing trend by increasing (α, β, γ). Physically, for $\alpha, \beta, \gamma \to 1$, the energy and momentum boundary layers become thinner as the value of the fractional parameters grows. Such physical impacts are due to the physical characteristics of the Mittag–Leffler function with three parameters of the Prabhakar derivative.

The study of how fluids behave when subjected to gravity in the domain of fluid dynamics is made via the Grashof number (Gr) and Hartmann number (Ha). Hartmann number is a connection between the viscous and buoyant forces. The impact of Gr is exhibited in Fig. 4a. The Grashof number tells us about buoyancy-driven convection. The raised value of Gr demonstrates that the buoyancy strength is larger than the diffusive and viscous effects. As the Gr is growing, strong thermal convection happens, prominent in enlarged mixing in the fluid and greater fluid flow near the heated sides. This is often seen in solar energy schemes, where temperature differences between heated surfaces and cooled air are the cause of a high value of Gr. Gaining more insight into how Gr affects fluid behaviour was crucial since it helps for the optimisation of intention parameters for solar energy schemes. This can lead to better proficiency through free convection.

Figure 4b displays the influence of Hartmann number Ha on the fluid flow. Hartmann number is linked to magnetic field-induced Lorentz forces. It is realised that fluid flow has exposed resistivity speedily in the boundary layer. This is because the higher magnetic effect increases the viscous effect between the fluid layers. So, this viscous effect decelerates the fluid flow.

The validation of different inverse numerical schemes for plate oscillating via $g(t) = te^{-\omega t}$ is observed in Fig. 5. All three inverse algorithms, *i.e.* Stehfest, Tzou, and Zakian, strongly overlap with each other, and this is evidence of validation of our results. The different base fluids can be used to make an effective NF for the considered system. The two changed base fluids, *i.e.* water and PVA, are used to check their efficiency in Fig. 6. This diagram is plotted to observe the behaviour of NF compared to ordinary fluid, and the plate is moved with $g(t) = e^{-\omega t}$. It is observed that the NF in the water shows higher thermal and flow performance than the PVA. So, water can be chosen instead of taking PVA as a base liquid.

The temperature and momentum profiles of the NF are observed in Fig. 7 at the different time values. The velocity by growing the estimation of time, the heat transfer, and velocity field are improved. Also, the velocity of the fluid is enhanced with time. The movement of fluid depends upon the movement of the plate. Three different graphs are plotted

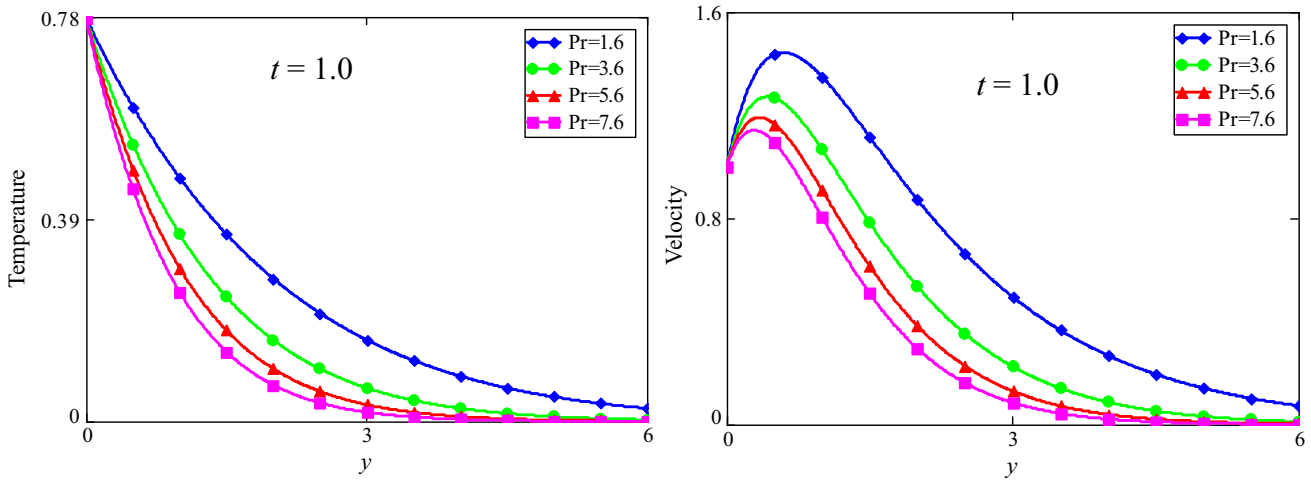

Fig. 1 Profiles of temperature and velocity for variations in Pr, when $g(t) = H(t)$.

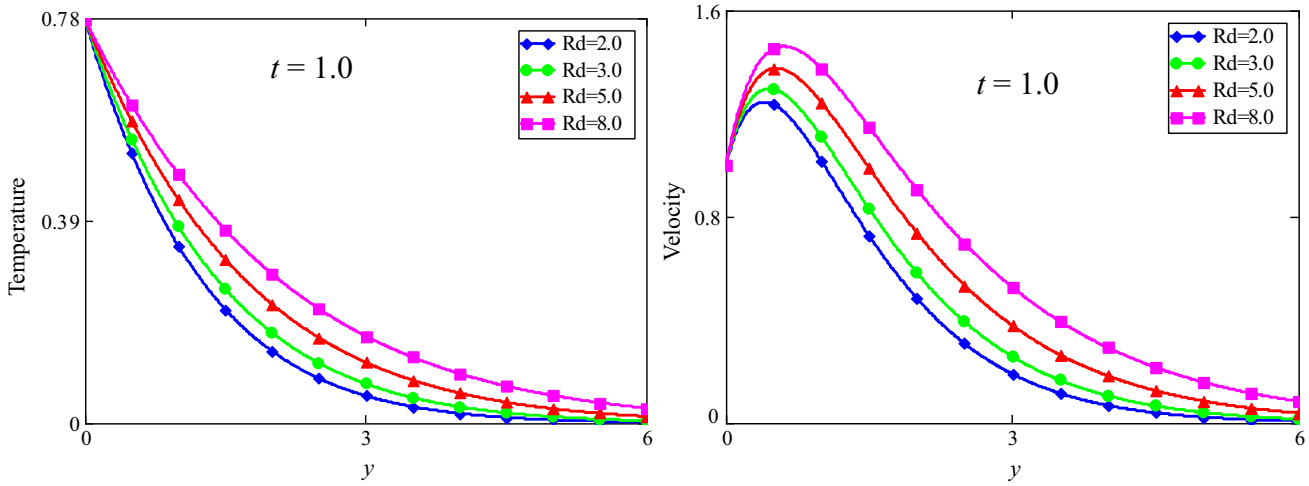

Fig. 2 Profiles of temperature and velocity for variations in Rd, when $g(t) = H(t)$.

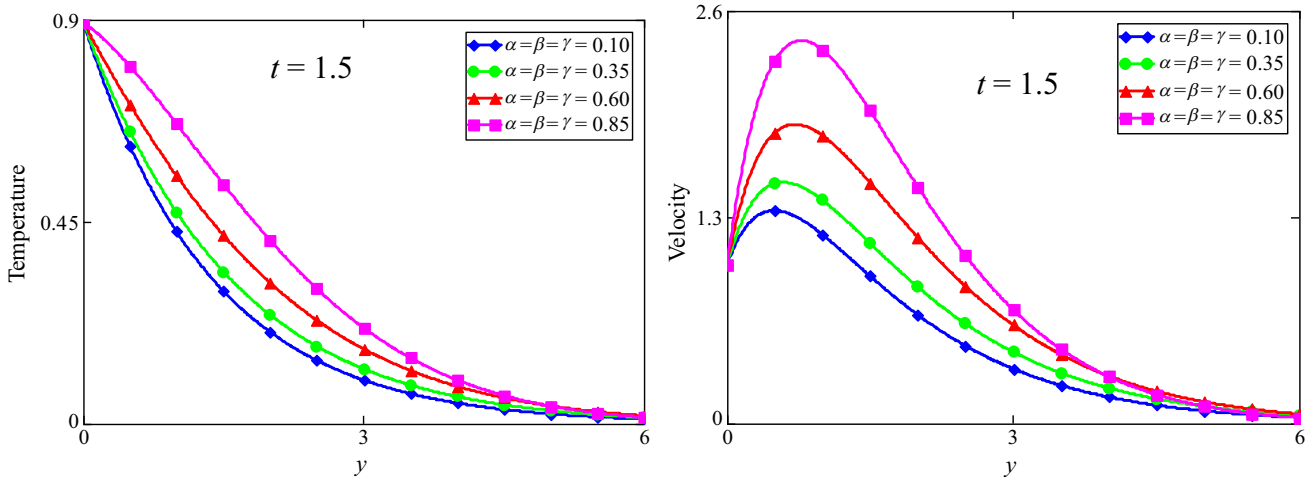

Fig. 3 Profiles of temperature and velocity for variations in fractional parameters (α, β, γ), when $g(t) = H(t)$.

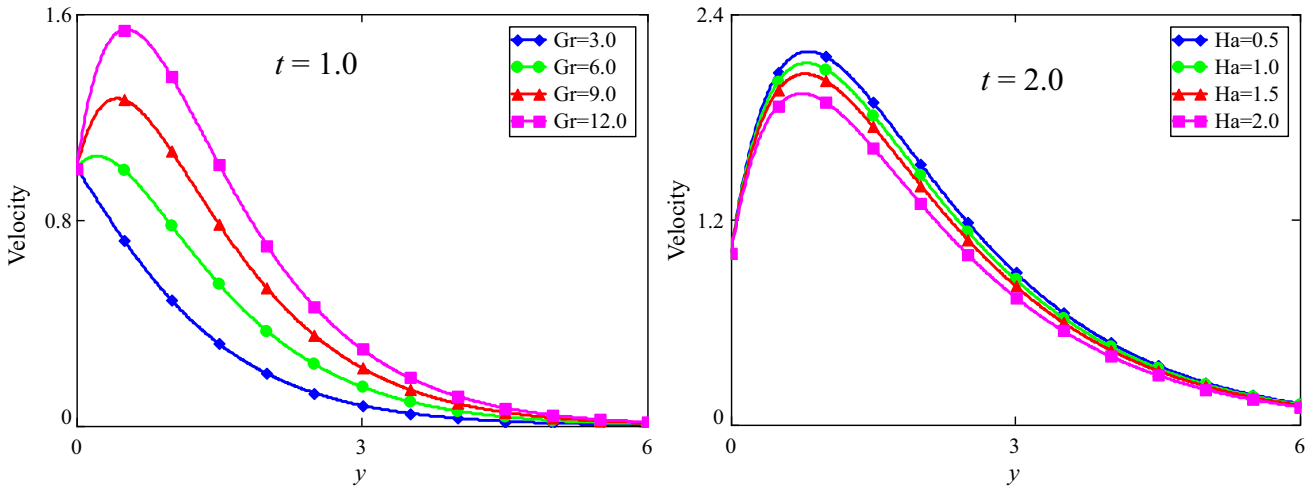

Fig. 4 Profiles of velocity due to a change in Grashof number (Gr) and Hartmann number (Ha), when $g(t) = H(t)$.

to visualise the behaviour of fluid movement with a velocity of the plate taken as $H(t), t$, and $e^{-\omega t}$. More movement is observed when the plate is moved by $e^{-\omega t}$. Table 1

Figure 8 demonstrates the comparison of our attained results with the study of *Riaz* et al. [10]. Here, fine solution precision between both results is detected. Tables 2–5 show the numerical investigations for momentum and temperature profiles, ordinary fluid, nanofluid, and Nusselt number for changed physical parameters by using three different numerical algorithms.

Revised analysis of conclusions (with applications)

The mixture of nanofluids in solar thermal structures is anticipated for several industrial thermal procedures. In this study, it is strongly claimed that employing NFs—principally graphene-based constructions—presents a significant alternative to boost solar energy capture and application in thermal engineering, industrial solar systems, and renewable energy schemes. The current investigation models the problem of refining the heat transmission capability of solar energy strategies, which is vital for applications such as photovoltaic thermal hybrid schemes, solar collectors, and

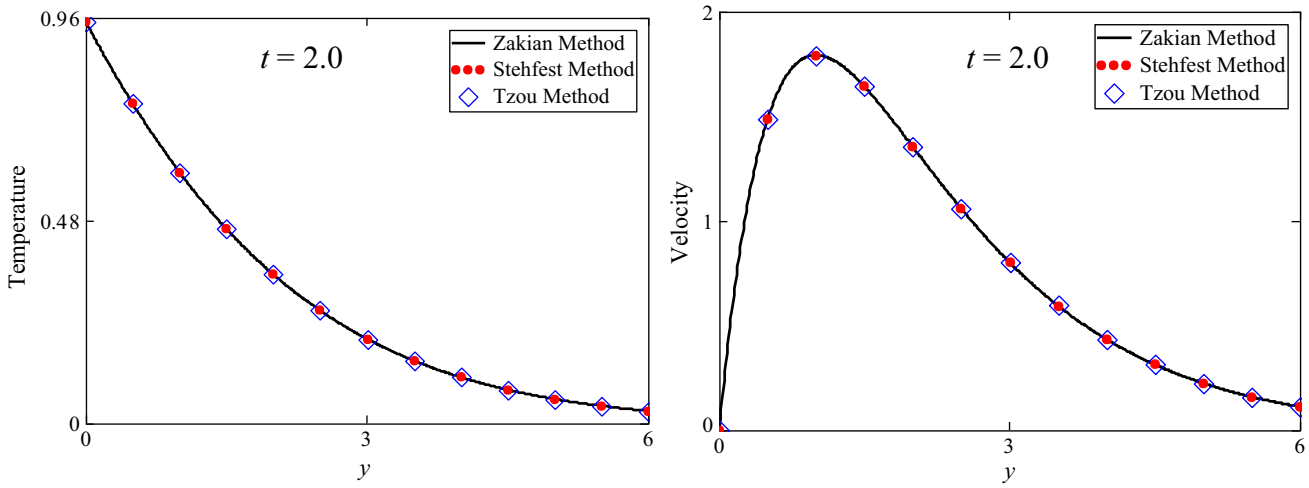

Fig. 5 Profiles of temperature and velocity for validations of the numerical inverse algorithms, when $g(t) = te^{-\omega t}$

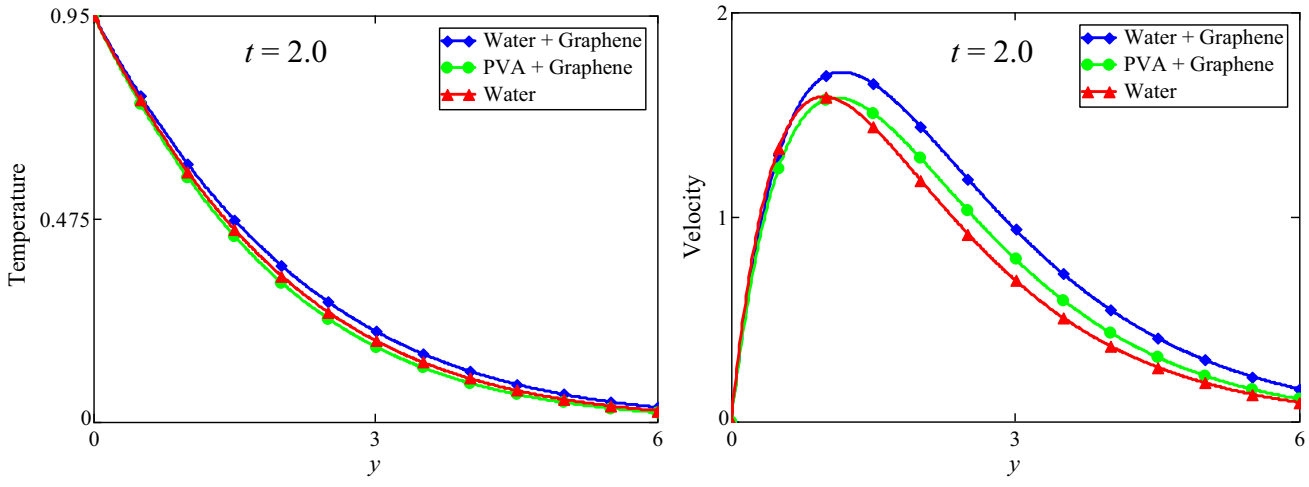

Fig. 6 Profiles of temperature and velocity for $g(t) = te^{-\omega t}$ Comparison of the change in base fluid, *i.e.* water and polyvinyl alcohol

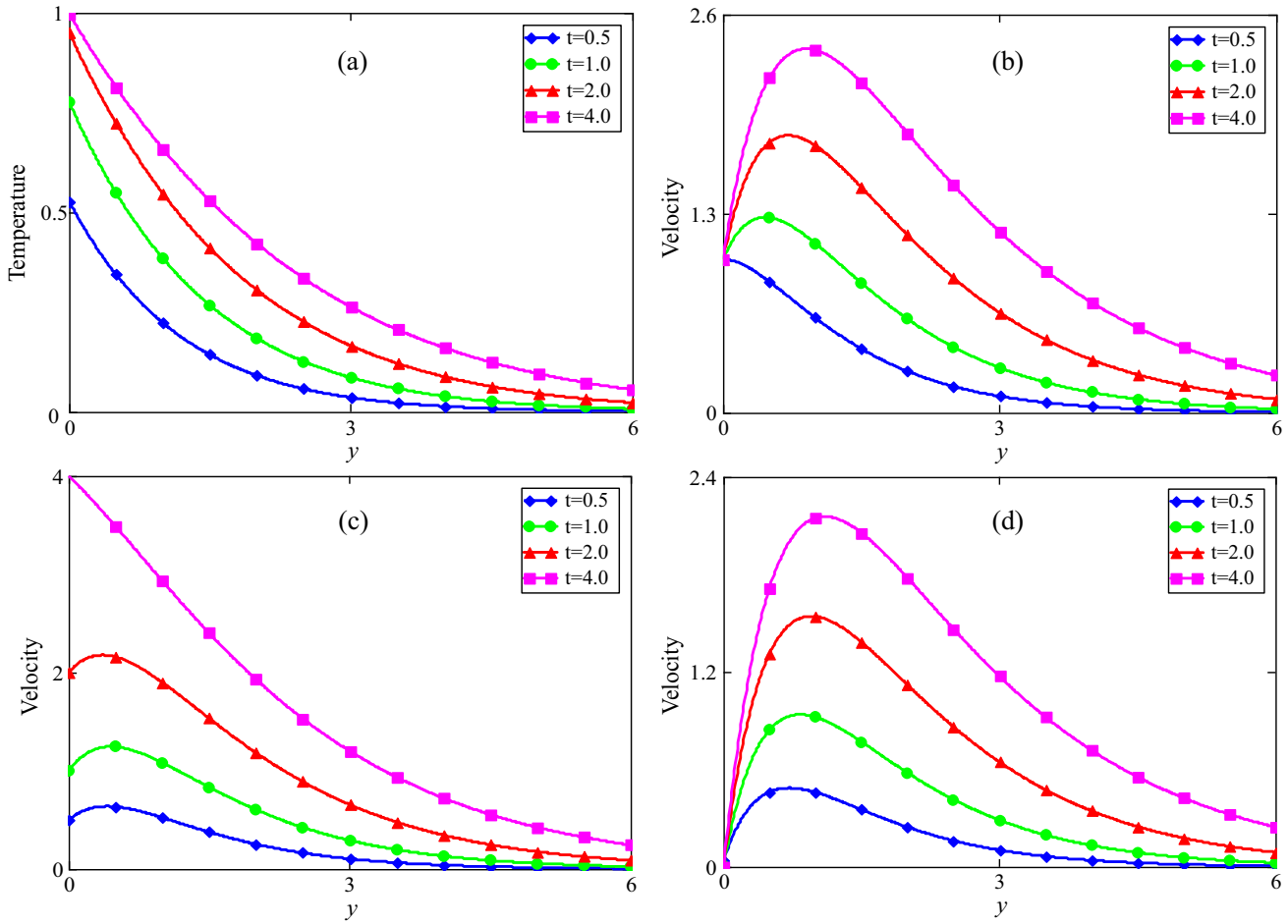

Fig. 7 Profiles of temperature and velocity variations due to change in values of time for movement with different functions when **(b)**-$g(t) = H(t)$, **(c)**-$g(t) = t$, and **(d)**-$g(t) = e^{-\omega t}$

concentrated solar power plants. The effects of diverse rheological parameters on the temperature and velocity curves of MHD Jeffrey-type NF (PVA/water + graphene) over a permeable moving heated plate are studied, with a special concentration on water-based graphene nanofluid. The Laplace scheme is employed to find the solution of the fractional model, which is based on the recently proposed Prabhakar derivative. Then, the inverse of this fractional model is found with the numerical approaches of Zakian, Tzou, and Stehfest for validation of results.

The key results are:

- The velocity is boosted due to the Grashof number, and it goes down due to the rise of the Hartmann number.
- The velocity and thermal fields go down while enlarging the Prandtl number.
- The temperature and momentum fields are enhanced by increasing the solar radiation parameter.
- The heat and flow profiles are enhanced due to the fractional effect at a large time value, but opposing interpretations are noted at a small time instant.
- The temperature and velocity profiles show an increasing trend for the water-based nanofluid, reflecting the suitability of water as a base fluid.
- By increasing the estimation of time, the heat transfer and velocity field are improved.

Table 1 Thermophysical characteristics of NPs and base fluids [39]

Physical characteristics	PVA	Water	Graphene
Density ρ/kg m^{-3}	1020	997.1	2250
Thermal conductivity κ/W m^{-1} K^{-1}	0.2	0.613	2500
Thermal expansion coefficient $\beta_T \times 10^{-5}/K^{-1}$	2.5	21	0.326
Specific heat capacity C_p/J kg^{-1} K^{-1}	2000	4179	2100

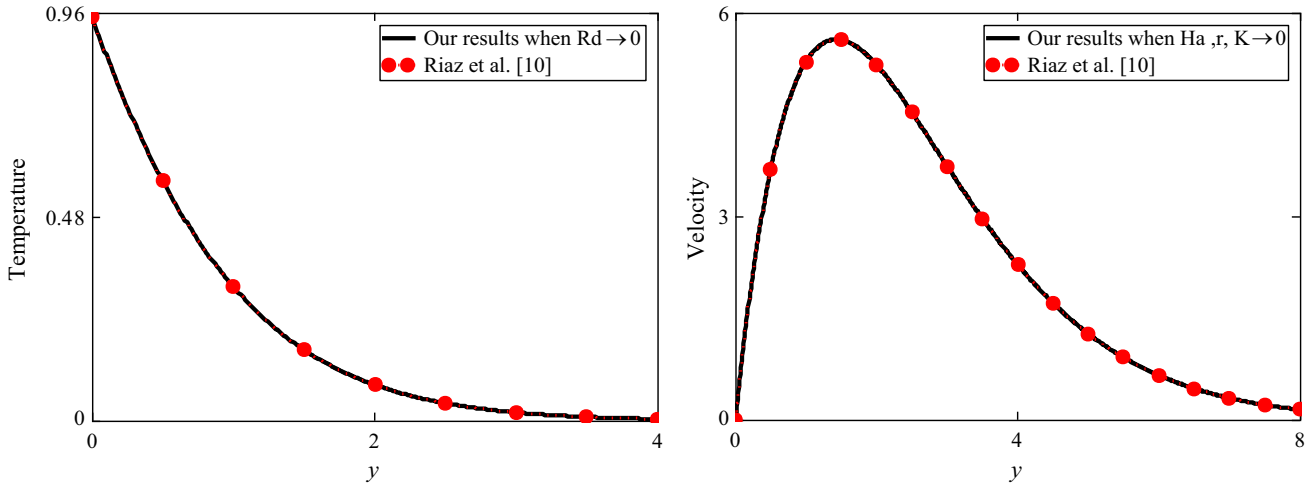

Fig. 8 Profiles of temperature and velocity for validations with Riaz et al. [10] when $g(t) = te^{-\omega t}$.

Table 2 Numerical investigation of Laplace inverse algorithms

z	Temperature by Stehfest	Temperature by Tzou	Temperature by Zakian	Velocity by Stehfest	Velocity by Tzou's	Velocity by Zakian
0.1	0.91046	0.91023	0.91042	0.42392	0.42375	0.42388
0.4	0.79809	0.79805	0.83432	1.2822	1.2823	1.2822
0.7	0.69611	0.69614	0.69603	1.7015	1.7017	1.7014
1.0	0.60431	0.60438	0.60426	1.8479	1.8482	1.8479
1.3	0.52231	0.52237	0.52227	1.831	1.8313	1.8309
1.6	0.44954	0.44961	0.44952	1.7217	1.722	1.7217
1.9	0.38537	0.38543	0.38536	1.5656	1.5659	1.5656
2.2	0.32562	0.32917	0.32911	1.3912	1.3915	1.3912
2.5	0.28004	0.2801	0.28005	1.2156	1.2159	1.2156
2.8	0.23747	0.23751	0.23747	1.0488	1.049	1.0488

Table 3 Numerical investigation of thermal and velocity fields for ordinary fluid and nanofluid for $t = 2.0$

z	Temperature for ordinary fluid $\varphi = 0$	Temperature for NF $\varphi = 10\%$,	% increase in temperature	Velocity for ordinary fluid $\varphi = 0$	Velocity for NF $\varphi = 10\%$,	% increase in velocity
0.1	0.90791	0.91042	0.28%	0.40905	0.37007	−9.53%
0.3	0.82724	0.83432	0.86%	0.98884	0.93082	−5.87%
0.5	0.75183	0.76287	1.47%	1.3323	1.3022	−2.26%
0.7	0.68164	0.69603	2.11%	1.5125	1.5317	1.27%
0.9	0.61657	0.63374	2.78%	1.5816	1.6563	4.72%
1.1	0.55646	0.57587	3.49%	1.5764	1.7042	8.11%
1.3	0.50113	0.52227	4.22%	1.5234	1.697	11.4%
1.5	0.45036	0.47278	4.98%	1.4409	1.6511	14.59%
1.7	0.40393	0.42721	5.76%	1.3417	1.5791	17.69%
1.9	0.36158	0.38536	6.58%	1.2347	1.4904	20.71%

Table 4 Numerical analysis of Nusselt number for $Rd = 0.5, t = 1.0$

γ, β, α	*Nu* for ordinary fluid $\varphi = 0$	*Nu* for nanofluid $\varphi = 10\%$	%age change in *Nu*
0.1	1.0592	1.2859	21.4%
0.2	1.0423	1.2653	21.39%
0.3	1.0098	1.2259	21.4%
0.4	0.96175	1.1675	21.39%
0.5	0.89911	1.0915	21.4%
0.6	0.82366	0.99988	21.39%
0.7	0.73746	0.89524	21.4%
0.8	0.64247	0.77992	21.39%
0.9	0.54032	0.65591	21.39%

Table 5 Numerical investigation of Nusselt number for different fractional parameters

α, β, γ	φ	*Pr*	*t*	*Rd*	Nusselt number
0.1	0.05	2.8	1.0	3.6	0.59674
0.3					0.56891
0.5					0.50653
	0.01				0.51209
	0.05				0.50653
	0.1				0.49911
	0.05	2.2			0.44899
		3.5			0.56632
		6.5			0.77177
		2.8	1.5		0.47505
			2.5		0.37154
			3.5		0.27983
			1.0	1.8	0.64243
				3.5	0.51194
				5.5	0.4282

- The Laplace inverse is investigated using Stehfest, Zakian, and Tzou's techniques, all of which demonstrate outstanding consistency with one another, which shows validations of our results.

Declarations

Conflict of Interests The authors declare that they have no known competing financial interests or personal relationships that could have appeared to influence the work reported in this paper.

References

1. Raza A, Thumma T, Khan SU, Boujelbene M, Boudjemline A, Chaudhry IA, et al. Thermal mechanism of carbon nanotubes with Newtonian heating and slip effects: a Prabhakar fractional model. J Indian Chem Soc. 2022;99(10):100731.
2. Garra R, Garrappa R. The Prabhakar or three parameter Mittag-Leffler function: theory and application. Commun Nonlinear Sci Numer Simul. 2018;56:314–29.
3. Giusti A, Colombaro I. Prabhakar-like fractional viscoelasticity. Commun Nonlinear Sci Numer Simul. 2018;56:138–43.
4. Alsharif AM, Abd Elmaboud Y. Electroosmotic flow of generalized fractional second grade fluid with fractional Cattaneo model through a vertical annulus. Chin J Phys. 2022;77:1015–28.
5. Rehman AU, Jarad F, Riaz MB, Shah ZH. Generalized Mittag-Leffler kernel form solutions of free convection heat and mass transfer flow of Maxwell fluid with Newtonian heating: Prabhakar fractional derivative approach. Fractal Fract. 2022;6(2):98.
6. Anwar T, Kumam P, Muhammad S. Comparative study on heat transfer performance of γAl2O3− C2H6O2 and γAl2O3− H2O nanofluids via Prabhakar fractional derivative model for MHD channel flows. Case Stud Therm Eng. 2022;38:102319.
7. Khan ZA, Shah NA, Haider N, El-Zahar ER, Yook SJ. Analysis of natural convection flows of Jeffrey fluid with Prabhakar-like thermal transport. Case Stud Therm Eng. 2022;35:102079.
8. Ali, Q., Khan, S. U., Amir, M., Adnan, & Waqas, M. (2024). Prabhakar fractional model for mixed convection flow of hybrid fluid in a channel with uniform walls. *Journal of Thermal Analysis and Calorimetry*, 1–12.
9. Ali, Q., Waqas, M., Mir, A., Alshammari, B. M., Amir, M., Khan, K. A., ... & Kolsi, L. (2024). Prabhakar fractional model for natural convection flow for kerosene oil based hybrid nanofluid containing ferric oxide and zinc oxide nanoparticles. *Case Studies in Thermal Engineering*, 104648.
10. Riaz MB, Rehman AU, Chan CK, Zafar AA, Tunç O. Thermal and flow properties of Jeffrey fluid through Prabhakar fractional approach: investigating heat and mass transfer with emphasis on special functions. Int J Appl Comput Math. 2024;10(3):111.
11. Hamzaoui M, Arsal M, Al-Khaled K, Farid S, Ali Q, Raza A, et al. Thermal transport of mixed convective flow of carbon nanotubes with Fourier heat flux model: Prabhakar-time derivatives assessment. Int J Mod Phys B. 2024;38(04):2450057.
12. Maatoug S, Al-Khaled K, Raza A, Labidi T, Kolsi L, Chammam W, et al. Fractional computations for free convective flow of Casson-hybrid nanofluid flow with sodium alginate and water as based materials. Int J Mod Phys B. 2024;38(18):2450240.
13. Raza A, Al-Khaled K, Muhammad T, Khan SU. Accelerating flow of carbon nanotubes with carboxymethyl cellulose and blood base materials with comparative thermal features: Prabhakar fractional model. Math Probl Eng. 2023;2023(1):3468295.
14. Ali, Q., Waqas, M., Mir, A., Alshammari, B. M., Amir, M., Khan, K. A., ... & Kolsi, L. (2024). Prabhakar fractional model for natural convection flow of kerosene oil based hybrid nanofluid containing ferric oxide and zinc oxide nanoparticles. *Case Studies in Thermal Engineering*, *60*, 104648.
15. Qadir, M. I., Majeed, U., ul Islam, F., Raza, A., Khan, S. U., Nazarova, N., ... & Khan, M. I. (2025). Enhanced heat transfer using nanofluids: a fractional Prabhakar derivative approach for Brinkman-type fluids. *Journal of Thermal Analysis and Calorimetry*, *150*(5), 3767–3775.
16. Acharya N. On the flow patterns and thermal behaviour of hybrid nanofluid flow inside a microchannel in presence of radiative solar energy. J Therm Anal Calorim. 2020;141(4):1425–42.
17. Sheikh NA, Ali F, Khan I, Saqib M. A modern approach of Caputo-Fabrizio timefractional derivative to MHD free convection flow of generalized second-grade fluid in a porous medium. Neural Comput Appl. 2018;30:1865–75.

18. Kataria HR, Patel HR. Effect of thermo-diffusion and parabolic motion on MHD second grade fluid flow with ramped wall temperature and ramped surface concentration. Alexandria Eng J. 2018;57(1):73–85.
19. Shah NA, Areshi M, Chung JD, Nonlaopon K. The New Semianalytical Technique for the Solution of Fractional-Order Navier-Stokes Equation. Journal of function spaces. 2021;2021(1):5588601.
20. Sene N. Fractional model and exact solutions of convection flow of an incompressible viscous fluid under the Newtonian heating and mass diffusion. J Math. 2022;2022(1):8785197.
21. Chu YM, Ikram MD, Asjad MI, Ahmadian A, Ghaemi F. Influence of hybrid nanofluids and heat generation on coupled heat and mass transfer flow of a viscous fluid with novel fractional derivative. J Therm Anal Calorim. 2021;144:2057–77.
22. Song YQ, Obideyi BD, Shah NA, Animasaun IL, Mahrous YM, Chung JD. Significance of haphazard motion and thermal migration of alumina and copper nanoparticles across the dynamics of water and ethylene glycol on a convectively heated surface. Case Stud Therm Eng. 2021;26:101050.
23. Jamshed W, Eid MR, Safdar R, Pasha AA, Mohamed Isa SSP, Adil M, et al. Retracted article: solar energy optimization in solar-HVAC using sutterby hybrid nanofluid with smoluchowski temperature conditions: a solar thermal application. Sci Rep. 2022;12(1):11484.
24. Khan, S. U., Sowayan, A. S., Riaz, S., Nadeem, M. S., & Ali, Q. (2024). Multiple slip nonlinear radiative bioconvective flow of nanofluid with variable thermal conductivity. *Numerical Heat Transfer, Part A: Applications*, 1–12.
25. Ali Q, Amir M, Metwally ASM, Younas U, Jan AZ, Amjad A. Investigation of MHD fractionalized viscous fluid and thermal memory with slip and Newtonian heating effect: a fractional model based on Mittag-Leffler kernel. J Therm Anal Calorim. 2024. https://doi.org/10.1007/s10973-024-13205-5.
26. Ali Q, Awan AU, Alassar RS, Amir M, Younas U, Farman M. Comprehensive study of tri-hybrid nanofluid flow in a vertical channel with Cu, Al2O3, and TiO2 nanoparticles via fractional dynamics and non-local kernel approach. Mod Phys Lett B. 2024. https://doi.org/10.1142/S0217984924504013.
27. Amir M, Ali Q, Raza A, Almusawa MY, Hamali W, Ali AH. Computational results of convective heat transfer for fractionalized Brinkman type tri-hybrid nanofluid with ramped temperature and non-local kernel. Ain Shams Eng J. 2024;15(3):102576.
28. Bilal M, Ali A, Mahmoud SR, Tag-Eldin E, Balubaid M. Fractional analysis of unsteady radiative brinkman-type nanofluid flow comprised of CoFe2O3 nanoparticles across a vertical plate. J Therm Anal Calorim. 2023;148(24):13869–82.
29. Sarwar N, Asjad MI, Almusawa MY. MHD rotating flow of a viscous fluid with heat sink and Prabhakar fractional derivative. Int J Mod Phys B. 2025;39(17):2550142.
30. Shanmugapriya M, Sundareswaran R, Gopi Krishna S, Fernandez-Gamiz U, Narasimman S. Magnetized Casson hybrid nanofluid flow under the influence of surface-catalyzed reactions over a porous moving wedge. AIP Adv. 2024. https://doi.org/10.1063/5.0216570.
31. Abro KA, Memon AA, Abro SH, Khan I, Tlili I. Enhancement of heat transfer rate of solar energy via rotating Jeffrey nanofluids using Caputo–Fabrizio fractional operator: an application to solar energy. Energy Rep 2019;5:41–9.
32. Raza A, Almusawa MY, Ali Q, Haq AU, Al-Khaled K, Sarris IE. Solution of water and sodium alginate-based casson type hybrid nanofluid with slip and sinusoidal heat conditions: a prabhakar fractional derivative approach. Symmetry. 2022;14(12):2658.
33. Ali Q, Riaz S, Memon IQ, Chandio IA, Amir M, Sarris IE, et al. Investigation of magnetized convection for second-grade nanofluids via Prabhakar differentiation. Nonlinear Eng. 2023;12(1):20220286.
34. Pantokratoras A, Fang T. Sakiadis flow with nonlinear Rosseland thermal radiation. Phys Scr. 2012;87(1):015703.
35. Cortell R. Fluid flow and radiative nonlinear heat transfer over a stretching sheet. Journal of King Saud University-Science. 2014;26(2):161–7.
36. Zakian V. Optimisation of numerical inversion of laplace transforms. Electron Lett. 1970;21(6):677–9.
37. Stehfest H. Algorithm 368: numerical inversion of laplace transforms [D5]. Commun ACM. 1970;13(1):47–9.
38. Tzou DY. Macro-to microscale heat transfer: the lagging behavior. John Wiley & Sons; 2014.
39. Obalalu AM, Oreyeni T, Abbas A, Memon MA, Khan U, Sherif ESM, et al. Implication of electromagnetohydrodynamic and heat transfer analysis in nanomaterial flow over a stretched surface: applications in solar energy. Case Stud Therm Eng. 2023;49:103381.